Principal axes of gene-regulated spatial organization of the human brain

Jacob W. Vogel[a,*]

[a]*Montreal Neurological Institute, McGill University, Montréal, QC, Canada*

Abstract

The human brain is characterized by a strong relationship between functional specialization and space. This relationship can be observed as a modular representation, where brain tissue self-segregates into structures and substructures with shared behavioral functions, as well as a gradient representation, where gradation in function appears to be organized systematically across specific linear axes. These principles of spatial-functional organization are ostensibly mirrored by, and perhaps regulated by, similar modular and graduated patterns of gene expression. Furthermore, both phenomena appear to be hierarchically organized, such that they can be observed globally across the whole brain, and locally within subregions. These relationships may be crucial for describing the complexity of neural organization, however, no study to date has directly analyzed the relationship between gene expression and physical (i.e. euclidian) space. I employ statistical cross-decomposition to identify patterns of gene expression that vary systematically along the rostral-caudal (y) and dorsal-ventral (z) spatial axes of the brain. Two robust modes of linear gene-space covariation were identified that together predicted the location of brain tissue samples with an average error of 12 mm. With a few notable exceptions (e.g. the parietal lobe), brain megastructures were clearly differentiated in space by the cross-decomposition model, and these global patterns significantly explained local spatial organization across most cortical and subcortical regions. These findings support the notion of mostly-linear molecular gradients as one of the central modes of topological organization of the brain, and specifically implicate two distinct and orthogonal axes as underlying aspects of this organizational structure.

*Corresponding authors: jacob.vogel@mail.mcgill.ca, alan.evans@mcgill.ca

1. Introduction

Spatial organization of the brain is extremely consistent within-species and demonstrates remarkable ontogenic conservation across species, indicating it to be a process regulated by gene expression during development. To this point, much research has characterized the role of genes regulating neuronal migration [1] and differentiation [2], and how these features contribute to neural development and organization. However, beyond simply documenting these phenomena, understanding the mechanisms regulating the spatial organization of the brain may be key to understanding brain function, as function itself seems to be organized systematically in space. This can be observed on a global level, where structures with distinct and highly modularized functions (e.g. the cerebellum) are also modularized in space, rather than distributed, and are themselves often subdivided into functionally distinct nuclei. Even within brain areas with a relatively homogeneous structure, function often varies across a local axis or axes in space. For example, neuronal connectivity patterns vary across dorso-posterior points of the human and macaque medial frontal cortex [3], the visual cortex harbors markedly different associative function as it radiates anterolaterally [4], and spatial functional divisions in, and even gradients through, space have been observed, most notably in the hippocampus [5, 6], but in other structures as well (e.g. [7, 8]).

The distribution of function through space has been particularly well documented in the hippocampus, and a number of studies have investigated genes that regulate this organization [9, 10, 11]. However, it remains unclear if such organizational patterns are unique within brain structures, or if they follow guiding principals observable throughout the brain. There are several lines of evidence for molecular gradients underlying the topographical organization of the brain at large. For example, a dual-origin hypothesis of the cerebral cortex has been proposed where dorsal and ventral aspects of the brain can be differentiated by cytoarchitecture and evolutionary expansion [12]. Additionally, a broad rostro-caudal pattern of gene expression has been observed in both the developing [13] and adult [14] human brain, which is accompanied by graduated variation in microarchitecture [15, 16]. While it is well established that gene expression is highly consistent within brain regions (i.e. is modular)[14, 17], this is not necessarily true for the cerebral cortex [16, 18]. In addition, brain-wide gene expression appears also to be hierarchical in its organization [14, 19], suggesting the possibility for a modular

molecular structure to coexist with large-scale molecular gradients.

The evidence presented builds a case for the existence of central axes of spatial organization to the brain, along which gene expression varies systematically, and even linearly. However, despite strong evidence for such phenomena, previous studies have not directly broached the relationship between patterns of gene expression and spatial organization. This question carries with it connotations not only about genomic regulation of the brain and how it relates to function, but also regarding how scientists conceptualize and represent the brain in space. Are our axes of anterior-posterior or dorsal-ventral simply orthogonal axes designed for convenience, or does the brain actually organize itself naturally along these axes, or others? To address this question, I leverage statistical cross-decomposition to explore patterns of systematic covariance between gene expression and space throughout the brain, and assess whether these global principles of organization are reflected locally within brain subregions.

2. Methods

2.1. Data

The Allen Human Brain Atlas is a dataset including >3,700 tissue samples extracted from the brains of six human donors. Each sample has undergone microarray analysis quantifying the gene expression for >58,000 probes targeting over 20,000 different genes [20]. Normalized gene expression data are provided for all probes across all samples, and approximate MNI coordinates of each tissue sample are also provided with the dataset. The coordinates given with the official dataset do not account for non-linear deformations [20], and so a different set of coordinates were used where these deformations and other sources of potential error were painstakingly accounted for (https://github.com/gdevenyi/AllenHumanGeneMNI). In addition, labels indicating which slab type (i.e. Cortex, Cerebellum or Brainstem) each sample was taken from were recorded, as well as more fine-grained labels indicating the exact anatomical structure each sample was extracted from.

Gene expression patterns differ across the six donors, which is to be expected due to the donors differing in age, sex and ethnicity. For the current analysis, I was not interested in individual differences, but rather common patterns of gene expression shared across humans. As such, donor effects were removed using regression. Specifically, for each probe, a model was

formulated such that expression across all tissue sample was set as the dependent variable, and five dummy coded variables representing donor ID were included as independent variables. The standardized residuals of this model were used for all further analysis, such that individual values represented gene expression normalized by full-brain expression levels and adjusted for donor.

The main variables used in this study are the normalized gene expression values and the corrected y and z coordinates representing sample location along the anterior-posterior and dorsal-ventral brain axes, respectively. x coordinates were not used due to the following reasons: i) the x- (right-left) axis is organizationally different from the y- and z-axes, because it is characterized by two (almost) mirrored hemispheres emanating from a central point. Efforts to address this would involve either moving all coordinates to one hemisphere, sacrificing potentially important information regarding hemispheric variation, or representing hemispheres separately, which would be severely limited by the proportionately lower number of samples extracted from the right hemisphere. ii) While there are a few exceptions (e.g. [21]), previous literature has focused much less on medial-lateral axis variation. iii) There is an added complexity in representation of the data in three dimensions, therefore, adding x information would simply be inconvenient from a visual standpoint. Due to the combination of these factors, x coordinates are not represented in our analysis, though future work may include this information. Please note that, for the sake of clarity, lower-case x,y,z will be used to refer to coordinates throughout the manuscript, whereas capitalized X and Y will be used to denote traditional independent and dependent variables in statistical analyses.

2.2. Statistical Analysis

All analyses were conducted using the scipy, numpy, scikit-learn, statsmodels, nilearn, nibabel, and pandas python libraries under Python version 3.6 inside a jupyter notebook (https://github.com/illdopejake/hack_projects/blob/master/CCA_GXP.ipynb). The primary analysis consists of utilizing cross-decomposition techniques to identify latent patterns of gene co-expression that demonstrate systematic linear covariance with spatial location (summary in Figure 1). This approach yields several advantages toward the study objectives. First, decomposition lends itself to representation of the high dimensionality of X, which is a 58,692 x 3702 matrix, and has been used effectively in previous gene-expression studies [22]. Second, entering

two orthogonal covariates (y and z coordinates) as Y allows for maximal interpretability, as "weights" or "loadings" on Y will essentially represent rotations to the y and z axes. Therefore, the "feature-space" created by latent variables resulting from cross-decomposition will be represented in Euclidian space, allowing for intuitive visualization and interpretation. Finally, the ultimate goal of the analysis is to ascertain the principal axes of spatial organization, and the decomposition of y and z coordinates can literally provide a "direction" of systematic gene expression, allowing for what is essentially a reconfiguration of the axes of locational representation in the brain.

The first step of the analysis involves reduction of X data using principal components analysis (PCA), where the first 100 components are retained [23] (Figure 1A). This step drastically increases the computation time necessary for subsequent analyses while still retaining most of the information contained in X. PCA is performed on the entire X dataset, unless where otherwise noted.

The central analysis is conducted in the following steps: i) model selection, ii) model evaluation and validation, iii) model description (summarized in Figure 1D).

2.2.1. Model selection

First, the model is split into a training and test set with a 75/25 split. To ensure the training and testing sample spanned a similar range of coordinates, the two samples were balanced so as to have an equal proportion of tissue samples from each anatomical structure label. 10-fold cross-validation is performed within the training sample only to determine the best choice of cross-decomposition estimator, as well as the optimal number of "modes" (correlations between latent X and Y variables) to fit. For most cross-decomposition algorithms, the maximum number of modes is equal to the matrix rank (in this case, only 2), but this is not the case for all algorithms. Three different algorithms were compared: partial least squares regression (PLSR; sometimes known as PLS2), canonical correlation (CCA) and canonical partial least squares (PLSC), sometimes known as PLS-C2A [24]. In the current context, PLSR is solved using the NIPALS algorithm, which is different from the SIMPLS algorithm implemented in some other software [25]. The most notable difference between these algorithms occurs at the deflation, where NIPALS loadings are calculated after deflation of the matrix. It should be noted that this implementation makes it possible not to explain 100% of the covariance between X and Y [26].

Ten-fold cross-validation was used to fit each estimator to the training

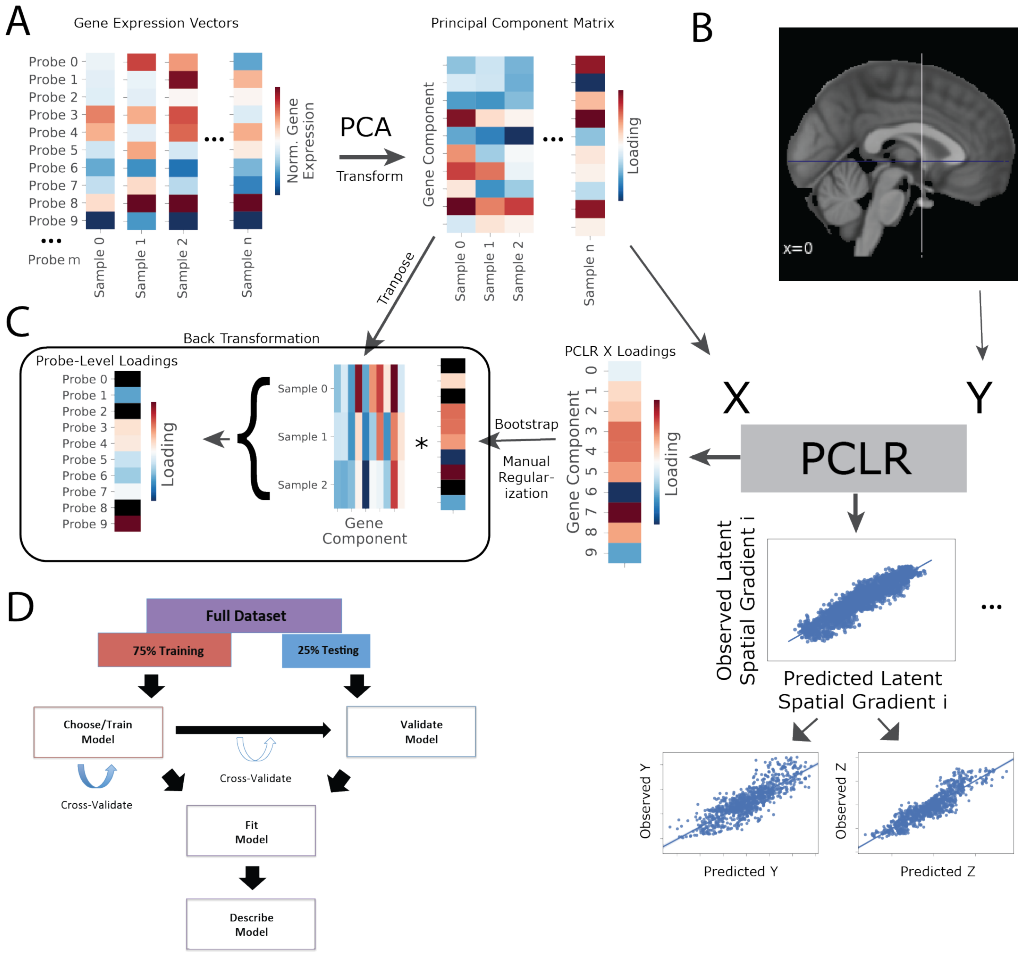

Figure 1: A) The full gene expression vector was reduced using PCA, and the transformed matrix was the X input of the PLSR model. B) y- and z- spatial coordinates representing the location of tissue samples were entered as the Y variables of the PLSR model. The model was used to generate modes of covariation, which were in turn used to predict y- and z-coordinates of unseen data. C) To characterize the latent X variable associated with each mode, the X loadings were transformed back into probe space by finding the dot product between the component matrix and the PCLR X loading vector. D) A schematic describing the overall analysis. The data was split into training (75%) and test (25%) sets. The training set was used to find the best estimator and number of modes, thorugh 10-fold cross-validation. As a validation, the optimal model was then applied to left-out training data, and this process was repeated 100 times. Finally, all the data was used to fit a final model, which was in turn evaluated and described.

data, and this process was repeated with the number of modes varying between 1 and 10. In all, 30 models were fit, each with 10-fold cross-validation. Model performance was judged on two metrics: r^2 score and mean absolute error. The former estimates explained variance of unseen data, while latter measures degree of unit error in prediction of unseen data. Note that in these cases, prediction is a summary across each mode – in other words, for each mode, X and Y are transformed to latent variables, correlated, and deflated. This is why the number of modes to extract is considered, as opposed to simply extracting all modes (e.g. [23]) . Note also that the prediction accuracy summarizes prediction of both elements of Y (i.e. y and z coordinates). The best (most accurate) combination of estimator and number of modes was used for all subsequent analysis. In this case, PLSR with 3 modes was selected (Fig. 2A). The third mode, while significant (see below), proved to be uninteresting, and thus it was not considered for subsequent analysis.

2.2.2. Model evaluation and validation

The best estimator and number of components diagnosed in the previous section was fit to the training data. Next, permutation tests were run to assess the likelihood of each mode occurring by chance. Specifically, the X data was permuted 1000 times, and for each permutation, the PLSR model was fit and the correlation of each mode recorded. Modes demonstrating r^2 values >95% of null models were considered to be significant, and this information was used to compute exact p-values.

Even if the PLSR model explains much of the variance in the data, the only way to validate this model is to apply it to unseen data. Therefore, the PLSR model fit to the training data was used to predict the 25% left out test data. Overall prediction accuracy for both y and z coordinates are reported. To ensure the results were not contingent on the specific train-test split, 100 train-test splits were performed and the mean and SD of predictions are reported. In addition, prediction accuracy of samples within each of the three slab types is also reported separately, which will give a sense of whether gene expression information taken from the whole brain can predict spatial location in separate brain aspects. As a comparison, six additional models were estimated and tested: two models were fit for each slab type, where one model involved X PCA-decomposition based on information from the whole brain (i.e. all samples) and one where PCA-decomposition was restricted to samples sharing the same slab type. The purpose of this analysis was to estimate how well global gene expression patterns predict spatial location as

compared to local gene expression patterns.

2.2.3. Model description

Once the model is validated successfully, the model can be fit once more to the entire dataset (i.e. both train and test) in order to utilize the most amount of data. The model was then used to predict (i.e. fit or describe) y and z coordinates for the entire dataset, and this fit was visualized. In addition, the fit was visualized separately for several anatomically distinct cortical structures. This was accomplished using the Desikan-Killiany atlas [27], where tissue samples were assigned to one of 34 bilateral cortical ROIs based on overlap of sample coordinates with the ROI label. The fit of y and z coordinates, respectively, were assessed separately for each ROI. P-values were generate using permutation test with 500 permutations per ROI. These p-values were subsequently corrected with false discovery rate (Q=0.05) for multiple comparisons, and an atlas was visualized labeling ROIs where the model significantly described variance in spatial location along the y coordinate, z coordinate, both, or neither. This analysis assesses whether whole brain gene expression patterns describe spatial organization within individual ROIs. Note that, due to the low number of sample within most ROIs, a train-test split could not be performed, and these analyses should be interpreted as purely descriptive.

2.2.4. Identifying latent components

While the performance of the PLSR model in predicting spatial organization is interesting, defining the latent variables contributing to the covariance may provide information pertaining to the biology underscoring the covariance. Therefore, latent X and Y variables were described. For Y, the y and z coordinates exist as orthogonal axes. Therefore, loadings are essentially rotations of these axes. The "latent" Y variables were therefore represented as rotations of y and z axes relative to a sagittal view of the brain.

For X, description of the latent variables was more convoluted due to the PCA and to the sheer number of probes associated with the original X matrix. First, confidence intervals were created around each of the 100 features (components) of X for each mode using bootstrapping (1000 iterations). P-values were created representing the probability that the loading value crosses 0. These p-values were then corrected using false discovery rate (Q=0.05) to determine features contributing "significantly" to the model. Loadings that were not significant were set to 0, creating a sort of manual L1 regularization.

Finally, for each mode, loadings for each individual probe were calculated by finding the dot product of the loading vector and the transposed component matrix from the original PCA (Figure 1C). This operation created a length 58,692 vector of loadings that, due to the imposed sparsity of the previous step, maintained a Laplace-like distribution. The probe loadings were interpreted in two ways: 1) Each sample was given a "score" based on the dot product of the gene-expression vector and the loading vector. This score represents the degree to which the sample expresses the pattern associated with spatial location. One would expect a linear gradient-like expression pattern of samples across the whole brain, directed in a manner suggested by rotations of Y described in the previous paragraph. 2) All probes were ranked based on their loading to the latent X variable and fed into the GOrilla gene set enrichment analysis (http://cbl-gorilla.cs.technion.ac.il/). This online tool takes an unthresholded gene set ordered by an effect of interest and uses leading edge analysis to identify Gene Ontology (GO) terms significantly enriched higher in the ranked list, corrected for multiple comparisons. Significantly enriched terms may provide clues as to shared biological functions and features that vary systematically with spatial organization. Because y and z coordinates are directions in space and have no instrinsic value, gene set enrichment was run once, and then run once more after the gene set was inverted. This provides information as to what functions are both "upregulated" and "downregulated" along the principal axis determined through the PLSR. Due to space limitations, only a handful of terms are reported.

3. Results and Discussion

Cross-decomposition was used to find patterns of gene-coexpression that covary along two-dimensional spatial gradients in the human brain. For computational purposes, the entire gene-expression matrix was decomposed with PCA into 100 components, which together explained 78.0% of the variance of the original matrix. A model selection routine suggested PLSR as the best estimator to represent this covariance, and this model was fit with three modes (Fig. 2A).

3.1. Cross-decomposition reveals patterns of gene expression that covary stably in space

A PLSR model fit to training data revealed three significant ($p<0.001$) modes of covariation, which explained 84.5%, 9.7% and 0.2% of the total

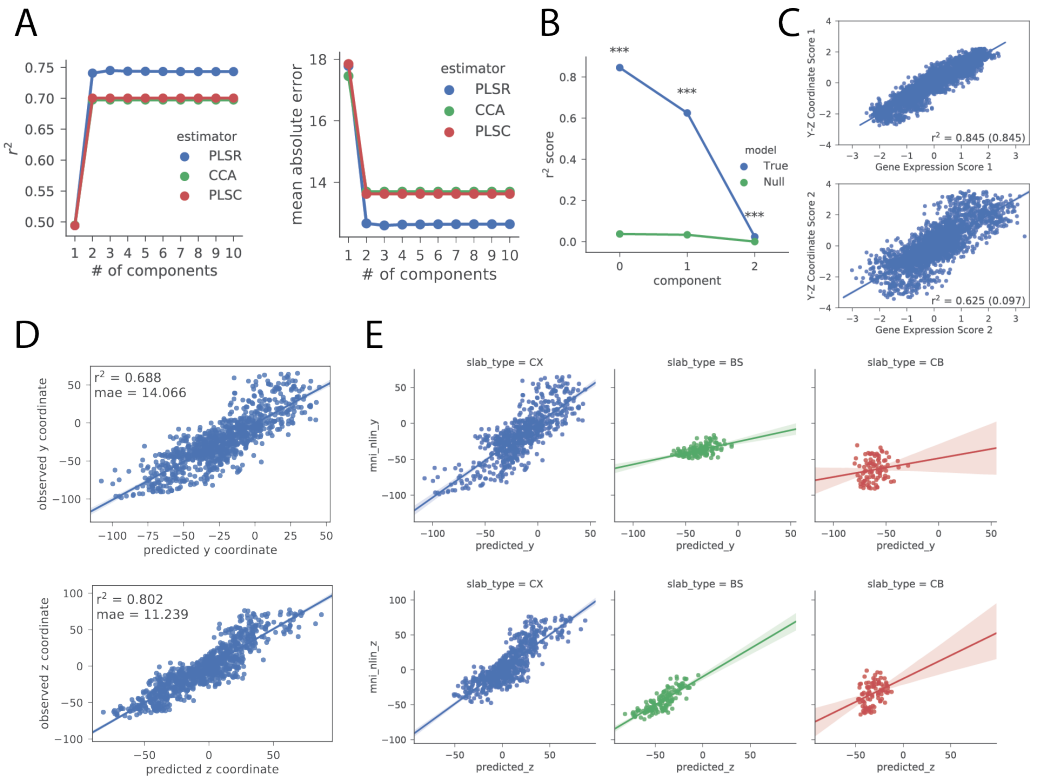

Figure 2: Model selection, evaluation and validation. (A) 10-fold cross-validation r^2 and error across estimators and components suggests PLSR with three modes to be the optimal choice. (B) Explained variance of the three modes of the PLS model fit to the training data, as well as the average explained variance of 100 null models. (C) Visualization of the first two modes. (D) Comparison of unseen observed y (top) and z (bottom) coordinates with coordinates predicted from the PLSR model. (E) Same as D but separated for different slab types. See Table 1 for statistics. PLSR = partial least squares regression; CCA = canonical correlation; PLSC = canonical partial least squares; CX = cerebral cortex; BS = brainstem; CB = cerebellum

model covariance, respectively (Fig. 2B,C). When applied to unseen test data, this model predicted y (r^2=0.69, MAE = 14.06) and z (r^2 = 0.80, MAE = 11.24) coordinates with a high degree of accuracy (Fig. 2D). This suggests samples were typically predicted to be around 12.5 mm from their actual location. These results were not contingent on the train-test split: 100 train-test splits revealed highly consistent results for both y (r^2: mean = 0.69, SD = 0.01; MAE: mean = 13.99, SD = 0.25) and z (r^2: mean = 0.80, SD = 0.01; MAE: mean = 11.17, SD = 0.24).

y coordinate	Cortex		Cerebellum		Brainstem	
	r^2	MAE	r^2	MAE	r^2	MAE
Global Model	0.64	15.4	0.02	14.4	0.27	7.5
Local Model (Global PCA)	0.66	15.1	0.23	10.8	0.68	3.2
Local Model (Local PCA)	0.74	13.05	0.42	9.3	0.76	2.7
z coordinate	**Cortex**		**Cerebellum**		**Brainstem**	
	r^2	MAE	r^2	MAE	r^2	MAE
Global Model	0.69	11.8	0.13	13.1	0.67	7.4
Local Model (Global PCA)	0.68	12.1	0.28	12.5	0.82	5.0
Local Model (Local PCA)	71.0	11.5	0.70	7.6	0.87	4.4

Table 1: Y coordinate prediction of unseen samples across models

3.2. Global gene expression patterns explain both local and global spatial location

Breaking down the predicted locations by slab type (i.e. cortex, brainstem or cerebellum) revealed overall poorer predictions within the cerebellum. Furthermore, predictions were poor for the y, but not z, coordinates of the brainstem (Fig. 2E, Table. 1). As a comparison, separate models were fit including only cortical, cerebellar or brainstem samples, and were each tested on unseen samples from the same slab. In addition, these models were repeated with local PCA decomposition, rather than transformed using information from the entire sample PCA. Cortical samples benefited marginally from local decomposition, while prediction of cerebellar samples was greatly improved by local decomposition, and prediction of brainstem samples was improved through within-slab model-fitting (Table. 1). Taken together, these results suggest that cerebellar and brainstem spatial organization are determined locally, but that a similar pattern of gene-expression organizes z-axis orientation of the cortex and brainstem.

After establishment of the stability of the PLSR model, one final PLSR model was fit across all data. The resulting model demonstrated similar properties to the model fit just to the training set: All three components occurred significantly greater than chance ($p<0.001$), and explained 84.8%, 9.5% and >0.001% of the total covariance, respectively. This full model explained the y (r^2=0.71, MAE = 13.7) and z (r^2=0.81, MAE = 10.9) coordinate data with a fair degree of accuracy, though the overall accuracy was barely improved compared to the model fit just to the training data. Fig 3A and B summarize

the prediction of all samples in space compared to the true spatial location. For predicted samples, coarsely defined structures can be observed centered relatively near their true location. A highly notable exception is the posterior parietal lobe, which was predicted to be nearly on top of the subcortex. In general, individual regions are predicted by the model to be clustered more tightly than they truly are, perhaps reflecting aforementioned strong regional autocorrelation an modular structure.

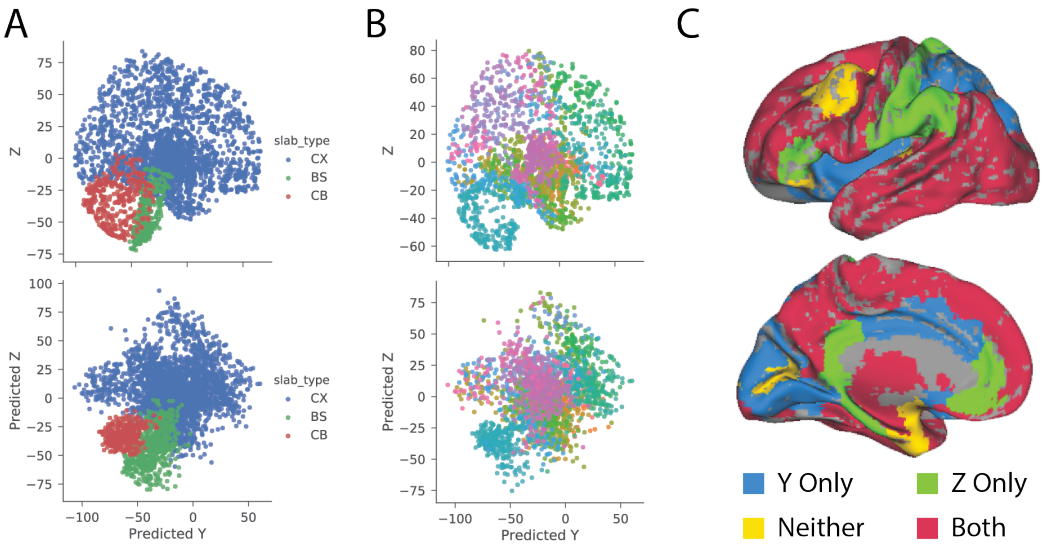

Figure 3: Description of brain spatial organization using gene expression. (A) Visualization of the true (top) and predicted (bottom) spatial y and z coordinates of all tissue samples, labeled by slab type. (B) The same, but this time labeled by anatomical ROIs. The labels are not shown, this visualization is to get a sense of how well the model predicted cerebral cortex organization. Note that the brainstem is not included. (C) A visualization of which cortical regions the model explained significant variance in for the y and/or z coordinate. CX = Cerebral cortex; CB = Cerebellum; BS = Brainstem

To establish whether global gene expression patterns can describe the spatial patterns of smaller subregions, model fit was observed within distinct cortical ROIs. Greater than chance fit was assessed using permutation tests, and results were corrected for multiple comparisons. Despite appearances, global gene expression patterns predicted a significant proportion of variance of both y and z coordinates in most cortical and all subcortical ROIs (Fig 3C). The model explained only y coordinates in the middle cingulate gyrus, medial occipital lobe (except primary visual cortex), insula, and superior parietal lobe, and explained only z coordinates in the parahippocampal gyrus, the retrosplenial and subgenual cortex, the angular gyrus, postcentral gyrus and

part of the dorsolateral prefrontal cortex. Finally, the model failed to describe spatial organization of the primary visual cortex, the entorhinal cortex and another part of the dorsolateral prefrontal cortex. It is possible that these regions are instead spatially organized along a medial-lateral axis (as has been described for the entorhinal cortex [21]), or that the organization of these structures differs generally from the rest brain.

3.3. The principal axes of human brain spatial organization are associated with specific gene expression patterning

The latent variables demonstrating covariance between gene expression and spatial location were characterized by examining their individual loadings (Fig 4).

The first mode, explaining >80% of the total covariance, demonstrated a near orthogonal clockwise rotation of y and z coordinates of nearly 40 degrees, such that it spanned from the cerebellum to the dorsomedial prefrontal cortex in the z direction, and from the midbrain to the precuneus in the y direction. This pattern explains why the posterior parietal lobes were poorly defined in Fig 3A and B, as the cortical gene expression of the first mode was fairly uniform, with the exception of the occipital lobe. However, the mode allowed for a clear gradient differentiating cerebellum, brainstem, midbrain/subcortex, occipital lobe, cerebral cortex as it moved positive to negative. It is also noteworthy that the first principal component represented the strongest weighted covariate, indicating this first mode to resemble the primary axis of variance in brain gene-expression. This mode was enriched for genes involved in regionalization, anterior/posterior pattern specification, embryonic skeletal system morphogenesis, embryonic organ morphogenesis, and pattern specification process (all Q<1e16), among many, many other processes. Regarding specific functions, the genes in this mode were heavily enriched for DNA-binding transcription activator activity, RNA polymerase II-specific (enrichment=14.2, FDR Q=8e13). Indeed, among the top 25 probes associated with this mode, 12 were homeobox (HOX) genes. Other genes of note in the top 25 included paired box 2 (PAX2), met proto-oncogene (MET), peripherin (PRPH) and neurodifferentiation 2 (NEUROD2). The inverse of the mode (i.e. more fronto-cortical regions) was specifically enriched for genes involved in anterograde trans-synaptic signaling (Q=5E-21), ion channel activity (Q=3e13), and neuron and synapse part (Q=7e27), particularly of the glutamatergic variety (Q=2e18). Genes of interest among the top 25 associated with the inverse of mode 1 included cortexin 3 (CTXN3),

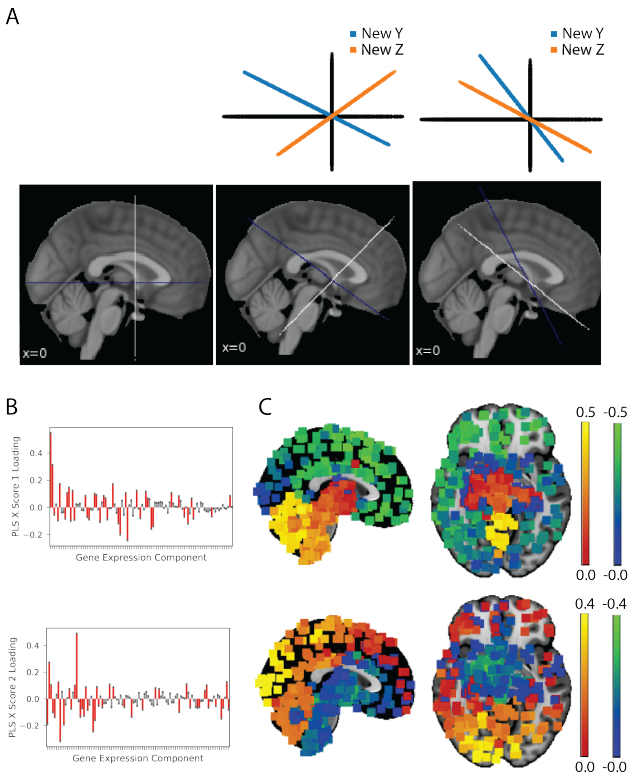

Figure 4: Characterizing the latent variables composing the PLSR modes (A) The latent Y variables representing spatial location for modes 1 (middle) and 2 (right) are visualized alone (top) and superimposed over a brain (bottom). Reference y and z axes are also visualized superimposed over a brain (left), and are visualized again as black lines in the top two subpanels. (B) Loadings for each of the 100 gene expression components for mode 1 (top) and mode 2 (bottom). Red bars represent loadings with weights significantly different from zero, assessed through bootstrapping and corrected for multiple comparisons. (C) Individual samples transformed by the latent X variable from mode 1 (top) and mode 2 (bottom) and superimposed over a brain in order to demonstrate the variation in mode loading through space.

neurogranin (NRGN), receptor (chemosensory) transporter protein 1 (RTP1) and guanine deaminase (GDA) and galanin prepropeptide (GAL).

The second mode, which accounted for an additional 10% of the whole model covariance, was primarily oriented on non-orthogonal axes that both spanned from the precuneus to subgenual cortex. The pattern differentiated brainstem and anteromedial cortical structures from the cerebellum and the rest of the cortex, and also clearly differentiated anterior from posterior parts of the cerebral cortex. This pattern also strongly resembled previously described partitions of the "dorsal" and "ventral" brain, putatively underlying directing and motivating behavior, respectively [12]. Interestingly, genes in

this mode were particularly enriched for potassium ion transport (Q=2e10) and voltage-gated cation channel activity (Q=3e15). Among the 25 genes associated with this mode were several genes previously identified to be associated with anterior-posterior structure differentiation, including transthyretin (TTR), parvalbumin (PVALB) and synaptotagmin II, as well as specific ion channels such as SCN1B and KCNS1. The inverse of mode 2 demonstrated a 50-fold enrichment of genes involved in embryonic skeletal system morphogenesis (FDR Q=3E11), and a 6-fold enrichment of ligand-gated ion channel activity (FDR Q=3e06). The top 25 genes associated with the inverse of mode 2 included 5 HOX genes.

4. Conclusion

Cross-decomposition was used to discover linear gradients in gene expression that explained the spatial structure of the brain. A pair of linear models based on gene expression could predict the location of a given brain sample within 12mm. Furthermore, these modes of gene expression proved to be gradients that naturally separated different megastructures, which were themselves organized in space. The first resembled the major component of general brain organization, distinguished major brain divisions, and was characterized by HOX genes and genes involved in spatial patterning. The second mode recapitulated the canonical "dorsal" and "ventral" brain, and separated brainstem, subcortical and frontal structures involved in motivated behavior and characterized by ligand-gated neurotransmitter systems, from cerebellar and posterio-dorsal structures involved in directed behavior and characterized by voltage gated ion channel systems. In general, global patterns of gene expression explained variance in local spatial organization, but this principal was far from absolute. Future work will need to better characterize local variation in gene-regulated spatial organization and how it relates to global patterns, and charaterize whether medial-lateral information can futher improve the prediction of tissue samples in space.

5. References

[1] K.-l. Guan, Y. Rao, Signalling mechanisms mediating neuronal responses to guidance cues, Nature Reviews Neuroscience 4 (2003) 941–956.

[2] N. Bertrand, D. S. Castro, F. Guillemot, Proneural genes and the specification of neural cell types, Nature Reviews Neuroscience 3 (2002) 517–530.

[3] S. Jbabdi, J. F. Lehman, S. N. Haber, T. E. Behrens, Human and Monkey Ventral Prefrontal Fibers Use the Same Organizational Principles to Reach Their Targets: Tracing versus Tractography, Journal of Neuroscience 33 (2013) 3190–3201.

[4] C. L. Colby, R. Gattass, C. R. Olson, C. G. Gross, Topographical organization of cortical afferents to extrastriate visual area PO in the macaque: A dual tracer study, The Journal of Comparative Neurology 269 (1988) 392–413.

[5] R. Vos de Wael, S. Larivière, B. Caldairou, S.-J. Hong, D. S. Margulies, E. Jefferies, A. Bernasconi, J. Smallwood, N. Bernasconi, B. C. Bernhardt, Anatomical and microstructural determinants of hippocampal subfield functional connectome embedding, Proceedings of the National Academy of Sciences 115 (2018) 201803667.

[6] I. K. Brunec, B. Bellana, J. D. Ozubko, V. Man, J. Robin, Z.-x. Liu, C. Grady, R. S. Rosenbaum, G. Winocur, M. D. Barense, M. Moscovitch, Multiple Scales of Representation along the Hippocampal Anteroposterior Axis in Humans, Current Biology 28 (2018) 2129–2135.

[7] C. Kelly, R. Toro, A. Di Martino, C. L. Cox, P. Bellec, F. X. Castellanos, M. P. Milham, A convergent functional architecture of the insula emerges across imaging modalities, NeuroImage 61 (2012) 1129–1142.

[8] W. M. Pauli, R. C. O'Reilly, T. Yarkoni, T. D. Wager, Regional specialization within the human striatum for diverse psychological functions., Proceedings of the National Academy of Sciences of the United States of America 113 (2016) 1907–12.

[9] E. Leonardo, J. Richardson-Jones, E. Sibille, A. Kottman, R. Hen, Molecular heterogeneity along the dorsalventral axis of the murine hippocampal CA1 field: a microarray analysis of gene expression, Neuroscience 137 (2006) 177–186.

[10] C. L. Thompson, S. D. Pathak, A. Jeromin, L. L. Ng, C. R. Macpherson, M. T. Mortrud, A. Cusick, Z. L. Riley, S. M. Sunkin, A. Bernard, R. B. Puchalski, F. H. Gage, A. R. Jones, V. B. Bajic, M. J. Hawrylycz, E. S. Lein, Article Genomic Anatomy of the Hippocampus, Neuron 60 (2008) 1010–1021.

[11] M. S. Bienkowski, I. Bowman, M. Y. Song, L. Gou, T. Ard, K. Cotter, M. Zhu, N. L. Benavidez, S. Yamashita, J. Abu-Jaber, S. Azam, D. Lo, N. N. Foster, H. Hintiryan, H.-W. Dong, Integration of gene expression and brain-wide connectivity reveals the multiscale organization of mouse hippocampal networks, Nature Neuroscience (2018).

[12] R. G. Giaccio, The dual origin hypothesis : An evolutionary brain-behavior framework for analyzing psychiatric disorders 30 (2006) 526–550.

[13] J. A. Miller, S. L. Ding, S. M. Sunkin, K. A. Smith, L. Ng, A. Szafer, A. Ebbert, Z. L. Riley, J. J. Royall, K. Aiona, J. M. Arnold, C. Bennet, D. Bertagnolli, K. Brouner, S. Butler, S. Caldejon, A. Carey, C. Cuhaciyan, R. A. Dalley, N. Dee, T. A. Dolbeare, B. A. Facer, D. Feng, T. P. Fliss, G. Gee, J. Goldy, L. Gourley, B. W. Gregor, G. Gu, R. E. Howard, J. M. Jochim, C. L. Kuan, C. Lau, C. K. Lee, F. Lee, T. A. Lemon, P. Lesnar, B. McMurray, N. Mastan, N. Mosqueda, T. Naluai-Cecchini, N. K. Ngo, J. Nyhus, A. Oldre, E. Olson, J. Parente, P. D. Parker, S. E. Parry, A. Stevens, M. Pletikos, M. Reding, K. Roll, D. Sandman, M. Sarreal, S. Shapouri, N. V. Shapovalova, E. H. Shen, N. Sjoquist, C. R. Slaughterbeck, M. Smith, A. J. Sodt, D. Williams, L. Zöllei, B. Fischl, M. B. Gerstein, D. H. Geschwind, I. A. Glass, M. J. Hawrylycz, R. F. Hevner, H. Huang, A. R. Jones, J. A. Knowles, P. Levitt, J. W. Phillips, N. Šestan, P. Wohnoutka, C. Dang, A. Bernard, J. G. Hohmann, E. S. Lein, Transcriptional landscape of the prenatal human brain, Nature 508 (2014) 199–206.

[14] M. J. Hawrylycz, E. S. Lein, A. L. Guillozet-Bongaarts, E. H. Shen, L. Ng, J. A. Miller, L. N. van de Lagemaat, K. A. Smith, A. Ebbert, Z. L. Riley, C. Abajian, C. F. Beckmann, A. Bernard, D. Bertagnolli, A. F. Boe, P. M. Cartagena, M. M. Chakravarty, M. Chapin, J. Chong, R. A. Dalley, B. D. Daly, C. Dang, S. Datta, N. Dee, T. A. Dolbeare, V. Faber, D. Feng, D. R. Fowler, J. Goldy,

B. W. Gregor, Z. Haradon, D. R. Haynor, J. G. Hohmann, S. Horvath, R. E. Howard, A. Jeromin, J. M. Jochim, M. Kinnunen, C. Lau, E. T. Lazarz, C. Lee, T. A. Lemon, L. Li, Y. Li, J. A. Morris, C. C. Overly, P. D. Parker, S. E. Parry, M. Reding, J. J. Royall, J. Schulkin, P. A. Sequeira, C. R. Slaughterbeck, S. C. Smith, A. J. Sodt, S. M. Sunkin, B. E. Swanson, M. P. Vawter, D. Williams, P. Wohnoutka, H. R. Zielke, D. H. Geschwind, P. R. Hof, S. M. Smith, C. Koch, S. G. N. Grant, A. R. Jones, An anatomically comprehensive atlas of the adult human brain transcriptome., Nature 489 (2012) 391–9.

[15] D. J. Cahalane, C. J. Charvet, B. L. Finlay, Systematic, balancing gradients in neuron density and number across the primate isocortex, Frontiers in Neuroanatomy 6 (2012) 1–12.

[16] A. Fornito, A. Arnatkevičiūtė, B. D. Fulcher, Bridging the Gap between Connectome and Transcriptome, Trends in Cognitive Sciences xx (2018) 1–17.

[17] Y. Ko, S. A. Ament, J. A. Eddy, J. Caballero, J. C. Earls, L. Hood, N. D. Price, Cell type-specific genes show striking and distinct patterns of spatial expression in the mouse brain, Proceedings of the National Academy of Sciences 110 (2013) 3095–3100.

[18] E. S. Lein, T. G. Belgard, M. Hawrylycz, Z. Molnár, Transcriptomic Perspectives on Neocortical Structure, Development, Evolution, and Disease, Annual Review of Neuroscience 40 (2017) 629–652.

[19] T. J. Nowakowski, A. Bhaduri, A. A. Pollen, B. Alvarado, M. A. Mostajo-Radji, E. Di Lullo, M. Haeussler, C. Sandoval-Espinosa, S. J. Liu, D. Velmeshev, J. R. Ounadjela, J. Shuga, X. Wang, D. A. Lim, J. A. West, A. A. Leyrat, W. J. Kent, A. R. Kriegstein, Spatiotemporal gene expression trajectories reveal developmental hierarchies of the human cortex, Science 358 (2017) 1318–1323.

[20] A. Arnatkeviciute, B. D. Fulcher, A. Fornito, A practical guide to linking brain-wide gene expression and neuroimaging data, bioRxiv (2018).

[21] A. Maass, D. Berron, L. A. Libby, C. Ranganath, Functional subregions of the human entorhinal cortex (2015) 1–20.

[22] R. Romero-garcia, K. J. Whitaker, J. Seidlitz, M. Shinn, P. Fonagy, R. J. Dolan, P. B. Jones, I. M. Goodyer, N. Consortium, E. T. Bullmore, E. V. Petra, NeuroImage Structural covariance networks are coupled to expression of genes enriched in supragranular layers of the human cortex 171 (2018) 256–267.

[23] S. M. Smith, T. E. Nichols, D. Vidaurre, A. M. Winkler, T. E. J Behrens, M. F. Glasser, K. Ugurbil, D. M. Barch, D. C. Van Essen, K. L. Miller, A positive-negative mode of population covariation links brain connectivity, demographics and behavior, Nature Neuroscience 18 (2015) 1–7.

[24] J. A. Wegelin, J. A. Wegelin, A Survey of Partial Least Squares (PLS) Methods, with Emphasis on the Two-Block Case (2000).

[25] S. de Jong, SIMPLS: An alternative approach to partial least squares regression, Chemometrics and Intelligent Laboratory Systems 18 (1993) 251–263.

[26] P. Geladi, B. R. Kowalski, PARTIAL LEAST-SQUARES REGRESSION: A TUTORIAL, Technical Report, 1986.

[27] R. S. Desikan, F. Ségonne, B. Fischl, B. T. Quinn, B. C. Dickerson, D. Blacker, R. L. Buckner, A. M. Dale, R. P. Maguire, B. T. Hyman, M. S. Albert, R. J. Killiany, An automated labeling system for subdividing the human cerebral cortex on MRI scans into gyral based regions of interest, NeuroImage 31 (2006) 968–980.